ACS APPLIED MATERIALS & INTERFACES

Forum Article

www.acsami.org

Influence of Semiconductor Thickness and Molecular Weight on the Charge Transport of a Naphthalenediimide-Based Copolymer in Thin-Film Transistors

Yevhen Karpov,[†] Wei Zhao,[‡] Ivan Raguzin,[†] Tetyana Beryozkina,[§] Vasiliy Bakulev,[§] Mahmoud Al-Hussein,[⊥] Liane Häußler,[†] Manfred Stamm,[†,∥] Brigitte Voit,[†,∥] Antonio Facchetti,*[,‡,#] Roman Tkachov,*[,†] and Anton Kiriy*[,†]

[†]Leibniz-Institut für Polymerforschung Dresden e.V., Hohe Straße 6, 01069 Dresden, Germany

[‡]Polyera Corporation, Skokie, Illinois 60077, United States

[§]Ural Federal University, Mira Street 28, 620002, Yekaterinburg, Russia

[∥]Center for Advancing Electronics Dresden (CFAED), Technische Universität Dresden, 01062 Dresden, Germany

[⊥]Physics Department, The University of Jordan, Amman 11942, Jordan

[#]Center of Excellence for Advanced Materials Research (CEAMR), King Abdulaziz University, P.O. Box 80203, Jeddah, Saudi Arabia 21589

Supporting Information

ABSTRACT: The N-type semiconducting polymer, P(NDI2OD-T2), with different molecular weights (MW = 23, 72, and 250 kg/mol) was used for the fabrication of field-effect transistors (FETs) with different semiconductor layer thicknesses. FETs with semiconductor layer thicknesses from ~15 to 50 nm exhibit similar electron mobilities (μ's) of 0.2–0.45 $cm^2\ V^{-1}\ s^{-1}$. Reduction of the active film thickness led to decreased μ values; however, FETs with ~2 and ~5 nm thick P(NDI2OD-T2) films still exhibit substantial μ's of 0.01–0.02 and ~10^{-4} $cm^2\ V^{-1}\ s^{-1}$, respectively. Interestingly, the lowest molecular weight sample (P-23, MW ≈ 23 kg/mol, polydispersity index (PDI) = 1.9) exhibited higher μ than the highest molecular weight sample (P-250, MW ≈ 250 kg/mol, PDI = 2.3) measured for thicker devices (15–50 nm). This is rather unusual behavior because typically charge carrier mobility increases with MW where improved grain-to-grain connectivity usually enhances transport events. We attribute this result to the high crystallinity of the lowest MW sample, as confirmed by differential scanning calorimetry and X-ray diffraction studies, which may (over)compensate for other effects.

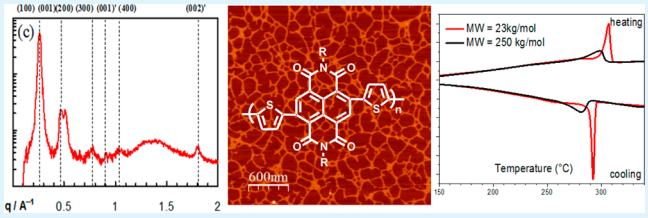

KEYWORDS: *semiconducting polymer, thin-film transistor, electron mobility, morphology, crystallinity*

INTRODUCTION

Semiconducting π-conjugated polymers have attracted considerable attention in recent years as an important class of materials for applications in large-area electronic devices, such as polymeric field-effect transistors (FETs).[1−6] Recent developments in material chemistry, physics, and device engineering have led to significant advances in FET performance and impressive mobilities for both holes (up to 14 $cm^2\ V^{-1}\ s^{-1}$)[7−9] and electrons (up to 6 $cm^2\ V^{-1}\ s^{-1}$).[10−12] To achieve such high mobility values, relatively thick semiconductor films in the 30–80 nm range are normally used. It is known however that in an FET charge carriers are confined by the gate field in a few nanometer-thick accumulation layer formed at the semiconductor–gate dielectric interface,[13] suggesting that the performance of ultrathin FETs may, in principle, approach that of much thicker devices. Ultrathin polymeric transistors would be of high technological interest for next-generation large-area electronics because using thin semiconductor films reduces material consumption. In addition, ultrathin transistors are of fundamental interest because, for the bottom-gate configuration, they enable direct probing of charge transport and film morphology with the aid of surface-sensitive techniques. Furthermore, high-quality ultrathin semiconductor layers may find applications in the fabrication of sensors and optically transparent devices.

Although transistors utilizing small molecules have been successfully downscaled into one-molecule-thick (monolayer) semiconductor channels,[14−17] fabrication of polymeric FETs with only a few molecular layers is far more challenging, and only a few examples have been demonstrated.[18,19] In general,

Special Issue: Forum on Polymeric Nanostructures: Recent Advances toward Applications

Received: November 7, 2014
Accepted: March 9, 2015
Published: March 17, 2015

DOI: 10.1021/am507759u
ACS Appl. Mater. Interfaces 2015, 7, 12478–12487

achieving highly performing FETs requires the presence of continuous pathways for charge carriers that extend throughout the whole semiconductor channel. This requirement is difficult to fulfill in ultrathin channel devices as this demands the formation of a large area two-dimensional (2D)-connected microstructure.[20,21] Previously, small-molecule based semiconducting monolayer FETs were prepared by a self-assembled monolayer technique.[17] A drawback of this process is that the self-assembly process is slow. Langmuir−Blodgett (LB)[18] and Langmuir−Schäfer (LS)[19] techniques were utilized for the fabrication of mono/multilayer FETs based on small-molecules and polymers, respectively; however, these methods may have limitations for scale-up. Polydiacetylene-based monolayer transistors were fabricated by solid-state polymerization of crystalline monomers; however, rather low FET performance was achieved in this case and this method lacks universality.[22,23] In view of this, fabrication of polymeric monolayer transistors using high throughput techniques would be a technologically attractive solution given the possibility of using the minimal amount of material, which can further reduce fabrication costs. Following this approach, Zhang et al. recently developed a new deposition method—on-the-fly dispensing spin-coating—which prevents unwanted dewetting of ultrathin semiconducting films on hydrophobic surfaces and allows the preparation of ultrathin films using a minimal amount of semiconductor materials.[23]

The bithiophene-naphthalene diimide copolymer (poly-{[*N*,*N*′-bis(2-octyldodecyl)-naphthalene-1,4,5,8-bis-(dicarboximide)-2,6-diyl]-*alt*-5,5′-(2,2′-bithiophene)} (P-(NDI2OD-T2))[10] is an n-type semiconductor.[24−32] This polymer shows remarkably high electron mobility both parallel and perpendicular to the substrate plane and a relatively weak dependence of charge transport on processing conditions and gate insulator dielectric constant, which are uncommon for several semiconducting polymers.[10,33−35] Furthermore, grazing-incidence wide-angle X-ray scattering (GIWAXS) studies of ∼50 nm thick P(NDI2OD-T2) films fabricated by spin-coating revealed a bulk unconventional face-on orientation of P-(NDI2OD-T2) molecules (with their π-stacking direction lying out-of-plane).[34] Indeed, other highly performing polymers, such as polythiophenes, as well as donor−acceptor copolymers, such as diketopyrrolopyrrole-[2a] and benzothiadiazole-based[8] copolymers, were found to exhibit a bulk edge-on orientation, supporting 2D charge transport in the $\pi-\pi$ stacking.[1−6] Following the discovery of P(NDI2OD-T2), several studies have attempted to rationalize charge transport in FETs and diode architectures based on this polymer[34,35] as well as investigate details of the film's morphology and how it varies with processing conditions and thermal history. A recent explanation for the efficient in-plane charge transport properties of P(NDI2OD-T2) thin films was proposed on the basis of near-edge X-ray absorption fine structure (NEXAFS) spectroscopy data.[36] By comparing the bulk-sensitive and surface-sensitive NEXAFS data, McNeil et al. observed[36] a molecular orientation at the surface of the film that was distinctly different from that of the bulk. Whereas a more "face-on" orientation of the conjugated backbone is observed in the bulk of the film, consistent with the lamella orientation observed by GIWAXS, a more "edge-on" orientation is observed at the surface of the film by surface-sensitive NEXAFS spectroscopy. This distinct edge-on surface orientation may also explain the high in-plane mobility that is achieved in top-gate P(NDI2OD-T2) FETs, whereas the bulk face-on texture accounts for the high out-of-plane mobilities that are observed in time-of-flight and diode measurements.[37] The observations described above raise interesting questions as to whether spin-coating can be used to fabricate ultrathin P(NDI2OD-T2) films, the morphology of the film, and how FET devices would perform by progressively reducing the P(NDI2OD-T2) film thickness.

In this work, we fabricated and evaluated the performance of FETs with semiconductor thicknesses systematically varied from ∼2 to 50 nm using three P(NDI2OD-T2) batches of different molecular weights. Two samples, indicated as P-23 with a MW ≈ 23 kg/mol and a polydispersity index (PDI) = 1.9 and P-250 with a MW ≈ 250 kg/mol and a PDI = 2.3, were synthesized by recently developed chain-growth polycondensation[38−57] catalyzed by a palladium complex ligated by bulky and electron-rich tri-*tert*-butylphosphine.[58] The commercially available P(NDI2OD-T2) with an intermediate molecular weight (MW = 72 kg/mol, PDI = 3.2), prepared by step-growth Stille polycondensation and designated here as P-72, was also investigated for comparison. The device performances were correlated to film morphologies studied by atomic force microscopy (AFM) and X-ray diffraction methods.

RESULTS AND DISCUSSIONS

Charge Transport Measurements. To minimize processing variations, we fabricated the polymer films in a glovebox by spin-coating 0.5−8 g/L *o*-dichlorobenzene (DCB) and tetrachloroethane ($C_2H_2Cl_4$) solutions, affording films with a nominal thickness of ∼2−50 nm (Table 1) as accessed by profilometry, optical absorption, and ellipsometry measurements (Figures S1 and S2 and Table S1 in the Supporting Information). The finished devices were then tested under ambient conditions. Representative transfer characteristics of these FETs are shown in Figure 1 and Figures S3 and S4 in the

Table 1. FET Parameters for P-23, P-72, and P-250 Based Devices Fabricated in this Study[a]

entry	polymer	solvent/conc. (g/L)	h^b (nm)	$\mu_{electron}$ (cm^2 V^{-1} s^{-1})	μ_{hole} (cm^2 V^{-1} s^{-1})
1	P-23	$C_2H_2Cl_4$/7	35−50[c]	0.30−0.46	∼0.008
2	P-23	$C_2H_2Cl_4$/3	16	0.31−0.37	∼0.001
3	P-23	$C_2H_2Cl_4$/1	5	∼0.005	∼0.0003
4	P-23	$C_2H_2Cl_4$/0.5	2.5	$\sim10^{-4}$	
5	P-72	DCB/8	50[c]	0.20−0.30	∼0.006
6	P-72	$C_2H_2Cl_4$/7	40[c]	0.27−0.33	∼0.009
7	P-72	$C_2H_2Cl_4$/3	15	0.27−0.28	∼0.007
8	P-72	$C_2H_2Cl_4$/1	5	0.01−0.015	∼0.001
9	P-250	DCB/8	50[c]	0.15−0.31	∼0.01
10	P-250	$C_2H_2Cl_4$/7	40[c]	0.10−0.30	∼0.009
11	P-250	$C_2H_2Cl_4$/3	14.5	0.10−0.20	∼0.006
12	P-250	$C_2H_2Cl_4$/1	4.5	0.01−0.02	∼0.001
13	P-250	$C_2H_2Cl_4$/0.5	2	$\sim10^{-4}$	

[a] W = 500 mm, L = 50 mm, C_i = 3.5−4.0 nF/cm^2. The carrier mobility was measured in saturation. The mobility range indicates the minimum and maximum values, whereas the approximate sign indicates the order of magnitude values considering the low drain currents. Performance range tested for at least 10 devices. [b] Film thickness on glass substrates as determined by optical absorption unless indicated (±10% accuracy). [c] Thickness of the active layer was determined by profilometry (±5% accuracy). Note, the films deposited from $C_2H_2Cl_4$ solutions are ∼3× thinner than those deposited from $CHCl_3$ as determined by AFM, optical absorption, and ellipsometry data (see Supporting Information).

DOI: 10.1021/am507759u
ACS Appl. Mater. Interfaces 2015, 7, 12478−12487

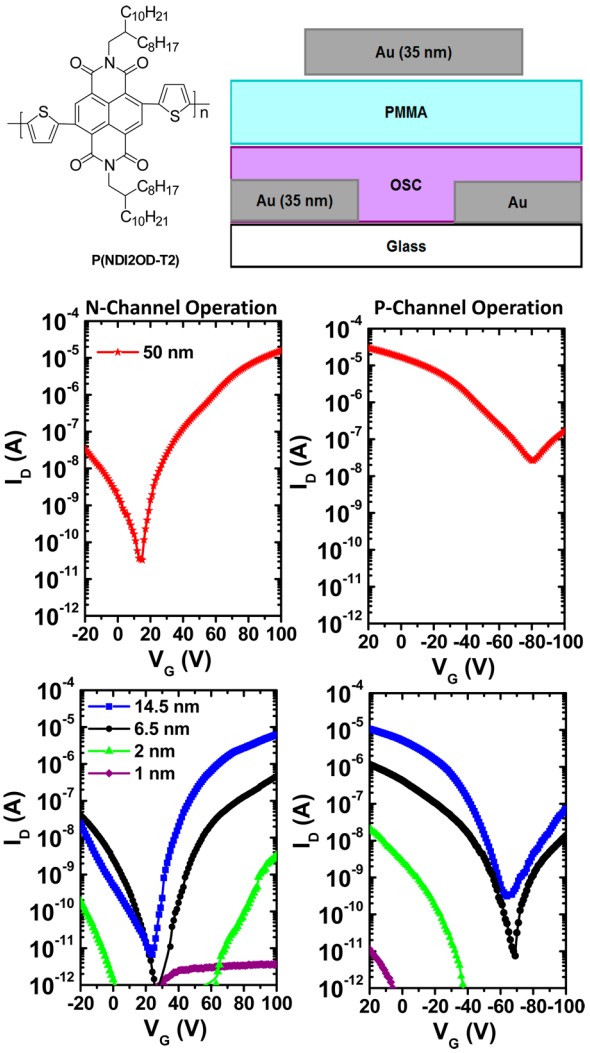

Figure 1. Polymer structure, schematic representation of the FET, and representative n- and p-channel transfer characteristics measured under ambient conditions for P-250 FETs with the indicated thicknesses. V_D = 100 and −100 V for n- and p-channel measurements, respectively. Gate leakage currents were omitted for clarity; however, they are ∼2−3 orders of magnitude lower than the drain currents at the maximum gate voltage for all well-behaving devices. Semiconductor film deposition details, except for the inactive ∼1 nm thick film, are shown in Table 1.

Supporting Information, and FET mobilities are collected in Table 1. FETs with the top-gate, bottom-contact configuration and 40−50 nm thick P-250 films fabricated on glass substrates with Au source/drain/gate electrodes and PMMA as the dielectric layer exhibit electron mobilities up to 0.31 $cm^2\ V^{-1}\ s^{-1}$ (0.01 $cm^2\ V^{-1}\ s^{-1}$ for holes) when measured under ambient conditions (Table 1, entries 9 and 10). The devices based on P-72 (commercial N2200, entries 1 and 2) exhibit saturation mobilities of 0.2−0.3 $cm^2\ V^{-1}\ s^{-1}$ for electrons and ∼0.006−0.009 $cm^2\ V^{-1}\ s^{-1}$ for holes (Table 1, entries 5 and 6), in agreement with previous studies.[3,12] Surprisingly, to a small yet statistically significant extent, the low molecular weight sample P-23 exhibits larger electron mobilities than those of higher MW P-72 and P-250 samples for 40−50 nm thick semiconductor films. Thus, the P-23 devices show saturation mobilities of 0.30−0.46 $cm^2\ V^{-1}\ s^{-1}$ for electrons and ∼0.008 $cm^2\ V^{-1}\ s^{-1}$ for holes (Table 1, Entry 1). This result is in contrast to previous studies in which low-MW polymers were found to exhibit poorer performance than the corresponding high-MW ones.[59−68]

Transistors based on much thinner semiconductor films were also fabricated by spin-coating all of the polymer samples. Several polymer concentrations were used for the film deposition as indicated in Table 1, affording films from ∼2 to 15 nm. The electron mobilities of the ∼15 nm devices are significant with values of 0.31−0.37 $cm^2\ V^{-1}\ s^{-1}$ for P-23 (entry 2), 0.27−0.28 $cm^2\ V^{-1}\ s^{-1}$ for P-72 (entry 8), and 0.10−0.20 $cm^2\ V^{-1}\ s^{-1}$ for P-250 (entry 11) (hole mobilities of ∼0.006−0.008 $cm^2\ V^{-1}\ s^{-1}$). Interestingly, these numbers are very similar to the electron/hole mobilities of the corresponding much thicker P(NDI2OD-T2) films.

For transistors with even thinner active layers, both the electron and hole mobilities decline when approaching the nominal submonolayer thickness (Table 1, entries 3, 4, 8, 12, and 13). Thus, transistors with an ∼5 nm thick semiconductor film continue to exhibit substantial electron mobilities (0.02−0.005 $cm^2\ V^{-1}\ s^{-1}$, entries 3, 8, and 12); however, those based on the high MW samples perform 2−3 times better than the FETs based on the low MW samples. Remarkably, transistors with the active layer thickness of ∼2 nm, somewhat lower than the monolayer thickness (the thickness of edge-on oriented PNDIT2 molecules is ∼2.5 nm), showed a measurable electron mobility of $\sim 10^{-4}$ $cm^2\ V^{-1}\ s^{-1}$ (Table 1, entry 13). However, further decreasing the semiconductor film thickness leads to full degradation of the FET performance. Interestingly, previously reported densely packed mono/multilayers of P(NDI2OD-T2) prepared by the LS technique with an exclusive edge-on orientation exhibited comparable electron mobilities.[22,23] Thus, it is quite impressive that our ultrathin and poorly compacted films (see AFM discussion) can afford such efficient transport characteristics. Furthermore, our P(NDI2OD-T2) ultrathin transistors exhibit charge carrier mobilities that compete with or surpass those of previously reported ultrathin films fabricated by dip-coating.[69]

The influence of the molecular weight of P(NDI2OD-T2) on the performance of transistors with different semiconductor thicknesses merits further discussion. In many cases documented in the literature, conjugated polymers with very high molecular weights (assuming they remain soluble) possess superior charge-transport, morphological, and film-forming properties, and therefore show better performance in thin film transistors than their low molecular weight counterparts. For example, remarkable hole mobility up to 10 $cm^2\ V^{-1}\ s^{-1}$ was recently reported for a high MW diketopyrrolopyrrole-based polymer, whereas the corresponding lower molecular weight polymers performed far more poorly.[8] Similar trends were observed for polybenzothiadiazoles[9] as well as other copolymers. From these precedents, the results of this work are somewhat surprising in view of the weak dependency of the carrier mobility on the polymer MW. To further investigate these trends, we carried out a detailed investigation of P(NDI2OD-T2) film morphology.

P(NDI2OD-T2) Film Morphology. Atomic force microscopy (AFM) is a powerful tool for studying polymers at the thin-film and single molecule levels.[70−72] Figure 2 shows AFM topography images of thin films prepared on silicon wafers by spin-coating solutions of P-250 and P-23 at concentrations varying from 0.01 to 1 g/L. Films prepared using 1 g/L (∼7 nm thick) had a uniform nanofibrous morphology (Figure 2a and i) similar to those previously observed for thin (25 nm)

DOI: 10.1021/am507759u
ACS Appl. Mater. Interfaces 2015, 7, 12478−12487

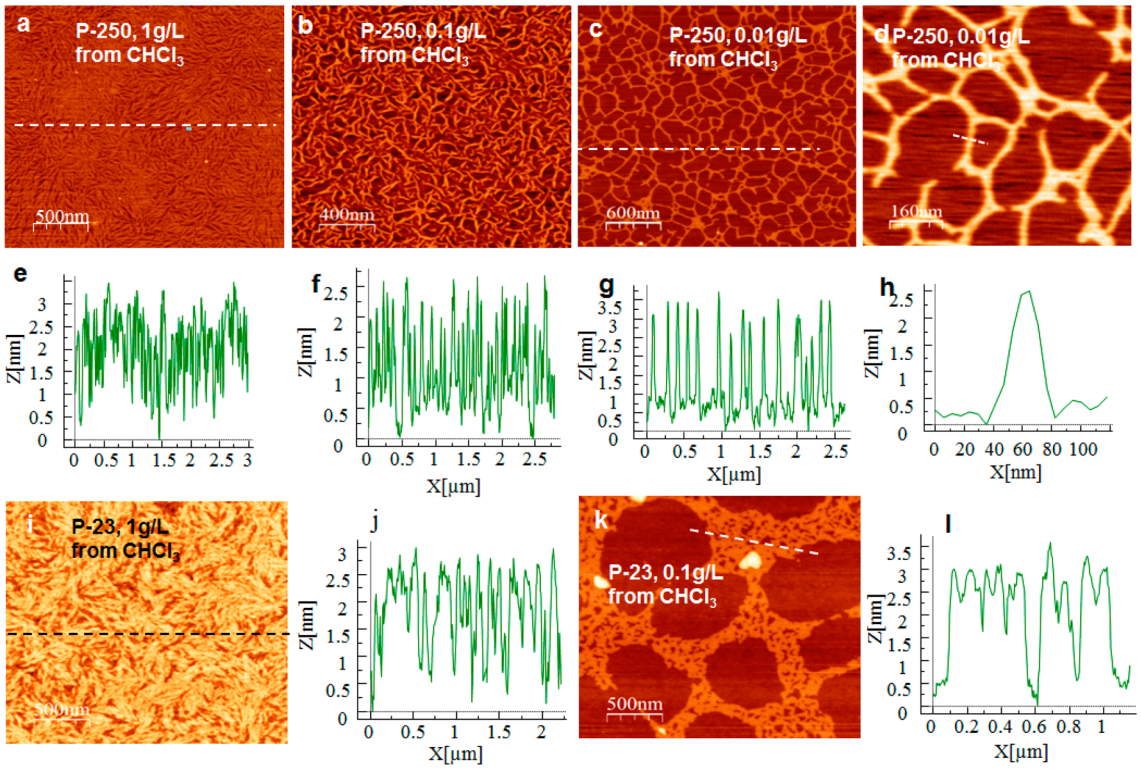

Figure 2. Representative AFM topography (a–d, i, k) images and cross sections (e–h, j, l) of P-250 (a–h) and P-23 (i–l) films spin-coated at 2000 r^{-1} on Si wafers from 1 g/L (a, e, i, j), 0.1 g/L (b, f, k, l), and 0.01 g/L (c, d, g, h) solutions.

P(NDI2OD-T2) films prepared by dip-coating[69] or thick (50–100 nm) P(NDI2OD-T2) films fabricated by spin-coating (Figure S5 in the Supporting Information).[10,37] Importantly, independent of the polymer molecular weight and solution concentration, the nanofibers in all of the samples exhibited essentially the same height (~2.5 nm, Figure 2c, f, i, and j). This thickness value is close to the computed molecular size of the edge-on oriented *N*-(2-octildodecyl)-substituted naphthalene diimide unit and to the lamellar *d*-spacing found for P(NDI2OD-T2) films.[69] The lateral width of the fibers was found to be ~30–40 nm (Figure 2d and h). It should be noted that the height of the elementary fibrils would be much smaller (<1 nm) if P(NDI2OD-T2) molecules adopted the face-on orientation. As such, the AFM data suggest that P(NDI2OD-T2) molecules deposited on our substrates (e.g., mica and Si wafers) at approximately monolayer thickness adopt the edge-on orientation. This is a reasonable arrangement because in this case P(NDI2OD-T2) molecules would expose the more hydrophobic alkyl side groups toward air, thus lowering the surface energy of the film. These data corroborate recently published NEXAFS spectroscopy data demonstrating that P(NDI2OD-T2) molecules in the very topmost layer have the edge-on orientation.[36]

The differences in the morphologies are obvious by analyzing the films deposited from the diluted polymer solutions. P-250 deposited from 0.1 and 0.01 g/L solutions (Figure 2b and c, respectively) forms uniform 2D networks (Figure 2b). In contrast, the network formed upon deposition of P-23 from 0.1 g/L solutions is far less uniform and are interwoven from smaller elementary fibers (Figure 2k). Furthermore, deposition of P-23 from even more dilute solutions (e.g., 0.01 g/L) fails to produce uniform films and instead results in disconnected and randomly located aggregates (not shown). Thus, it may be assumed that for ultrathin films a uniform 2D network as formed from the higher MW P-250 sample should exhibit better charge transport than the disconnected film morphology of the P-23 film. This data is fully consistent with the FET data for ultrathin (≤5 nm) films. On the basis of literature reports[7−9] and taking into account general considerations about efficient charge percolation of 1D conductors, the high MW P-250 polymer sample should perform much better than the others, especially for ultrathin-based devices. However, despite the order of magnitude difference in MW, P-250 FETs performed only slightly better in the monolayer transistor configuration than those based on low MW P-23. Furthermore, for the thick film devices, P-23 displayed statistically higher mobility, which may be related to different crystallinities of the samples. To quantify film crystallinity, we carried out differential scanning calorimetry (DSC) and X-ray diffraction measurements for these two P(NDI2OD-T2) samples as discussed below.

Thermal Analysis. The thermal properties of P-23 and P-250 were investigated by DSC. Heating–cooling–heating cycles were performed to achieve a comparable thermal history of the samples. Both polymer samples are crystalline (Figure 3); however, P-23 shows a slightly higher crystallinity than P-250, which follows from the melting enthalpy (Table 2).

The much sharper melting peak of P-23 is due to the lower dispersity index of P-23 and its less entangled structure as a consequence of its smaller molecular contour length. Importantly, the lower MW sample has even higher melting and crystallization temperatures as well as a higher melting enthalpy than the high MW sample. These data indicate that the lower MW P-23 sample studied in this work has already reached the saturation regime of the melting temperature versus molecular weight dependence. As further evidence,

DOI: 10.1021/am507759u
ACS Appl. Mater. Interfaces 2015, 7, 12478–12487

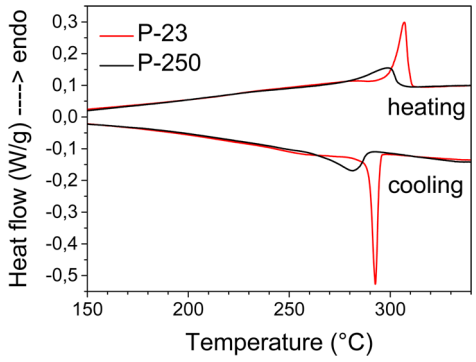

Figure 3. DSC curves of P-23 (red lines) and P-250 (black lines).

Table 2. DSC Data on Polymers P-23 and P-250

	first heating		cooling		second heating	
polymer	ΔH_m [a] (J/g)	T_m [c] (°C)	$T_{c,o}$ [b] (°C)	$T_{c,m}$ [c] (°C)	ΔH_m [a] (J/g)	T_m [c] (°C)
P-23	24.3	312.5	294.8	292.6	18.5	306.9
P-250	21.5	310.2	276.9	286.8	14.9	294.9

[a] ΔH_m is the transition melting enthalpy. [b] $T_{c,o}$ is the extrapolated onset of crystallization. [c] T_m and $T_{c,m}$ are the peak maximum temperatures.

Figure S5 in the Supporting Information shows a DSC curve for a far lower MW P(NDI2OD-T2) sample (P-9) within which the crystallization of this low molecular weight sample is shown to be hindered. The first heating run shows a small cold crystallization at 130 °C ($\Delta H_{c,c}$ = 0.5 J/g) and melting at 143 °C (ΔH_m = 1.0 J/g). During cooling and the second heating run, the polymer stayed in an amorphous state (glass transition temperature T_g = 71 °C). To conclude, the higher melting temperature of P-23 relative to P-250 can be explained in terms of lower entanglement of the shorter polymer chains, which provides enhanced $\pi-\pi$ staking interactions and thus contributes to its higher crystallinity.

X-ray Diffraction. To further probe the morphology of P(NDI2OD-T2) samples, we prepared free-standing P-250 and P-23 films with thicknesses of ~100 nm by drop-casting and investigated X-ray incidents perpendicular to the films. Compared to films prepared by spin-coating, drop-casted films in which the polymers have time to reorganize should provide a better picture of the intrinsic capability of the polymers to crystallize. Panels a and b in Figure 4 show 2D XRD patterns of free-standing films of both polymers. The corresponding radially averaged diffraction patterns are shown in Figure 4c and d, respectively. The intensities in Figure 4a and b are uniformly distributed on circles in accordance with an isotropic distribution of crystallites in the plane of the samples. Clearly, the (100) reflection due to lamellar stacking is present for both films up to the fourth order. However, P-23 film reflections exhibit higher intensities and narrower widths as compared to the corresponding reflections of the P-250 film.

The (100) lamellar stacking peak positions lie at q ~ 0.26 $Å^{-1}$ (lamellar spacing d ~ 24 Å) for both polymer films. The broad hump from q ~ 1.1 to 2.0 $Å^{-1}$ is attributed to amorphous scattering from disordered side chains. The two reflections at q ~ 0.47 and 0.91 $Å^{-1}$ are attributed to two polymorphs

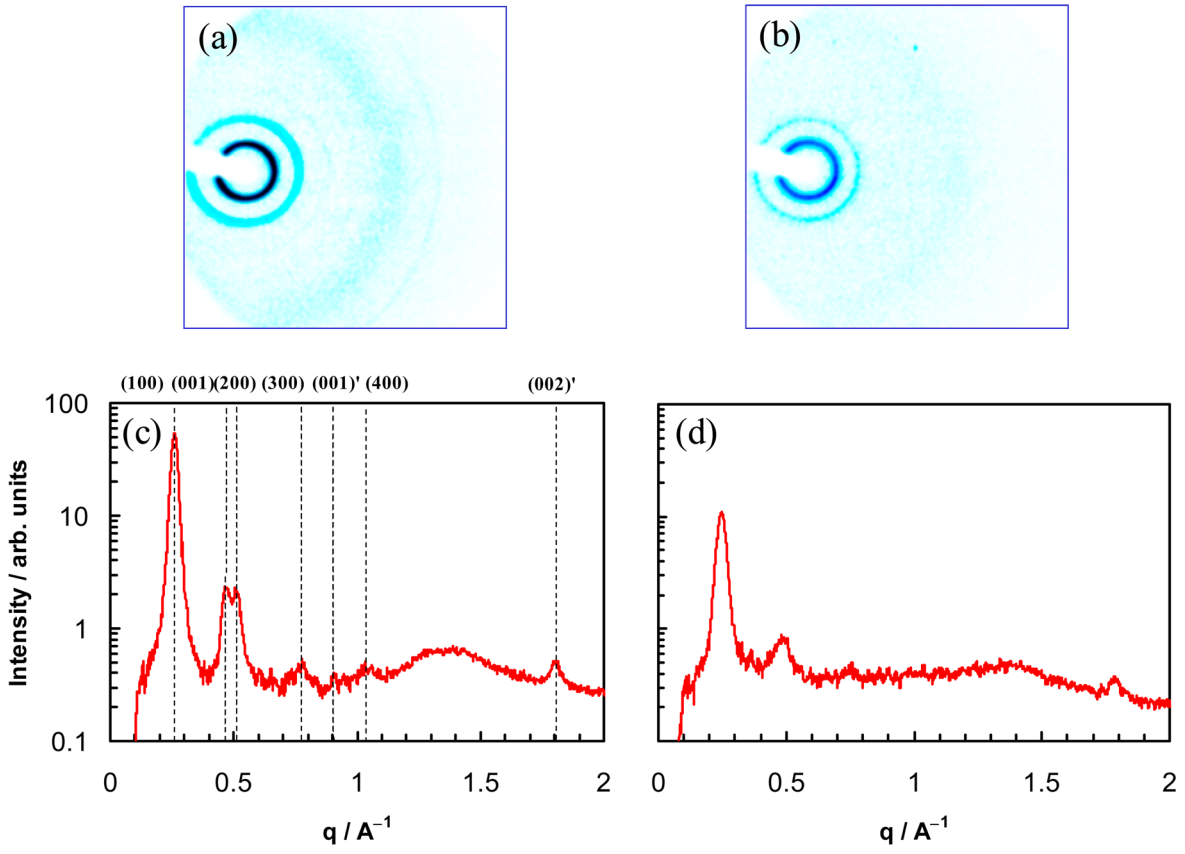

Figure 4. Two-dimensional X-ray diffraction patterns obtained with the beam perpendicular to the free-standing film of the (a) P-23 and (b) P-250 polymers along with the respective radially averaged patterns of the (c) P-23 and (d) P-250 polymers.

DOI: 10.1021/am507759u
ACS Appl. Mater. Interfaces 2015, 7, 12478−12487

associated with the repeating unit in the (001) and (001′) series, respectively.[10−15]

To obtain more quantitative data, we extracted the relative degree of crystallinity, χ, and the coherence length of the above samples from the XRD curves. The whole curve was fit using individual Gaussian functions for each diffraction peak, and the broad amorphous hump was superimposed on a linear background. χ values were obtained from the ratio of the total scattering intensity of the (100) peak to that of the amorphous hump. The coherence length was extracted from the full width at half-maximum, fwhm, of the (100) peak (2π/fwhm), and the results are summarized in Table 3. As can be seen, the data indicate that there is an overall higher population and larger correlation length of the crystallites in the low MW film, which can be attributed to higher crystallinity of the P-23 sample.

Table 3. Relative Degree of Crystallinity, χ, and Coherence Length of P-23 and P-250 Derived from XRD Data

	χ (%)	coherence length (nm)
P-23 film	80	41
P-250 film	59	23

Thus, the XRD diffraction measurements show that the lower molecular weight P-23 material exhibits a higher tendency for lamellar crystallization in agreement with the DSC data. In addition, GIWAXS diffraction measurements performed for 50 nm-thick films of P-23 and P-250 show that the crystallites in both films predominantly adopt an orientation where the (100) or side-chain stacking direction is perpendicular to the substrate normal (Figure S7 in the Supporting Information). However, P-23 exhibits a significantly higher tendency for lamellar crystallization than P-250. These data further suggest that the higher electron mobility of P-23-based FETs at film thicknesses of 15−50 nm may be due to its higher crystallinity relative to P-250. This crystallinity effect could compensate for the usual MW effect observed for other polymers (namely, that higher molecular weight polymers exhibit higher mobility).

However, there are no fundamental discrepancies between this work and prior literature findings. In general, for efficient charge transport, a sufficient number of continuous (preferably defect-free) pathways for carriers must be developed in the transistor channel spaning from the source to the drain. The charge transport through individual polymer chains usually does not limit overall macroscopic charge transport[73] if the chains do not contain structural defects (e.g., if they are planar and do not contain chain kinks or chemical defects that interrupt π-conjugation). In these cases, the charge transport is limited by hopping from one chain to another, and it is optimized by (1) improved chain order, (2) tightly packed chains (shorter $\pi-\pi$ distance), and (3) longer chains. From these considerations, increasing the molecular weight favors charge transport because it decreases unfavorable chain-to-chain hopping events, and it increases attractive $\pi-\pi$ staking interactions between chains. However, these factors do not necessary lead to higher crystallinity. Flexibility/motion of the polymer chains during film preparation, which is in general different for different polymers, is the factor that may strongly affect the molecular weight/crystallinity dependence described above. Indeed, when the polymer contour length significantly exceeds its persistence length, the polymer chain may kink, twist, fold, and entangle with other chains during film formation, thus leading to disruption of π-conjugation and reduction of crystallinity, which in turn deteriorates charge transport.[73] Hence, the "mobility versus MW dependence" may follow different trends depending on the polymer structure because the final result is a superposition of several factors acting at the molecular (chain flexibility, π-stacking), morphological (texturing, crystallinity), and film-forming (wetting, film continuity) property levels. Furthermore, the "mobility versus MW dependence" may be very complex even for a given polymer if the molecular weight varies considerably. In addition, it may depend significantly on the route of preparation. For example, as shown by Müllen et al, for benzothiadiazolo (PCDT-BTZ)-based polymers with solubilizing linear alkyl chains, the highest MW samples exhibited both the greatest crystallinity and the highest hole mobility in FETs.[8] The same trend was observed for diketopyrrolopyrrole-based polymers studied by Ong et al.[7] Although P(NDI2OD-T2) does not follow this trend, and the lower MW sample exhibited higher mobility, it displays the highest crystallinity. Thus, analyses of the literature data and our work suggest that "higher crystallinity results in higher mobility" can be a more important trend than "higher molecular weight results in higher mobility". However, it must be emphasized that this is also not necessarily a universal trend, because many other factors, including interactions with the surface, solvent, and substrates, as well as details regarding orientation and morphology, can be equally important. Because of the polycrystalline nature of most π-conjugated polymer films, the charge transport between crystalline domains (grains) strongly affects the overall charge transport and, under certain circumstances, this becomes a limiting factor.[74] This correlation is especially valid for small molecules, well-defined oligomers and polymers with very low molecular weights, and having very narrow polydispersity.[59−68] For example, very low molecular weight regioregular P3HT (Mn = 2.4 kg/mol)[60] and PCDT-BTZ with branched solubilizing chains (Mn = 1.8 kg/mol)[8] exhibit crystallinity that is higher than that of their higher MW counterparts, but they exhibit low FET mobilities. Nevertheless, our low MW sample, P-23, has a much higher MW than typical π-conjugated polymers and therefore it does not fall into the true low MW regime. This result is clearly supported by the DSC analysis. Thus, our samples belong to a MW regime where film crystallinity is the main factor affecting charge transport efficiency, a result that is fully consistent with the XRD and FET measurements.

CONCLUSIONS

In this work, we investigated P(NDI2OD-T2) field-effect transistors with variable thicknesses (from ∼1 to 50 nm) and molecular weights (from 25 to 250 kg/mol) of the semiconducting layer. Devices with conventional 35−50 nm semiconductor thicknesses exhibited electron mobilities of 0.2−0.45 $cm^2\ V^{-1}\ s^{-1}$, in agreement with previous studies. Interestingly, decreasing the P(NDI2OD-T2) layer thickness to ∼15 nm did not lead to any significant degradation of transistor performance (0.1−0.4 $cm^2\ V^{-1}\ s^{-1}$). Further reduction of the active film thickness led to reduced performances; however, FETs with semiconductor films as thin as ∼5 nm continued to exhibit substantial electron mobilities up to 0.02 $cm^2\ V^{-1}\ s^{-1}$. Remarkably, even ∼2 nm thick P(NDI2OD-T2) layer devices, which is an active layer thickness that is somewhat lower than the nominal monolayer thickness, showed a measurable

DOI: 10.1021/am507759u
ACS Appl. Mater. Interfaces 2015, 7, 12478−12487

electron mobility of ~10^{-4} cm^2 V^{-1} s^{-1}. Interestingly, for thicker semiconductor films (15−50 nm), FETs based on the lowest molecular weight sample, P-23, exhibited statistically higher electron mobilities than those based on the highest MW, P-250. This result is due to the highly crystalline nature of the lowest MW sample, as confirmed by differential scanning calorimetry and X-ray diffraction studies, which can (over)-compensate for other MW effects. On the other hand, devices based on thinner films (5 nm) exhibit the opposite transport behavior with high MW-based devices performing 2−4× better than those those fabricated with low MW samples. This trend is rationalized by the ability of the high MW sample to form a highly interconnected network of bundled polymer chains, which are clearly accessed by the AFM images in Figure 2, and span the whole channel transistor surface. Therefore, for ultrathin films, poor film continuity and morphology of the low-MW sample overcome its intrinsic capability to crystallize. Thus, our work indicates that controlling the polymer architecture at the molecular level enables us to finely tune the transport efficiency over a broad range of semiconductor film thicknesses.

EXPERIMENTAL SECTION

Materials. Synthesis of P-23 and P-250 was reported previously.[19] P-72 was synthesized at Polyera Corp. following the procedure reported in ref 3a, and it is commercially available as Activink N2200. All other chemicals for synthesis were purchased from Aldrich and used as received.

Differential Scanning Calorimetry. DSC was carried out with a DSC Q 1000 TA instrument in the temperature range of −60 to 350 °C under nitrogen atmosphere at a scan rate of 10 K/min. All samples were investigated in a heating−cooling−heating cycle. The glass transition temperature was determined using the half step method, the maximum melting peak, extrapolated onset temperature, and maximum of the crystallization process were calculated along with their corresponding transition enthalpies.

XRD. Two-dimensional transmission XRD measurements were performed using a Bruker D8 Discover diffractometer operating at 1.6 kW. The diffractometer is equipped with a Cu Twist tube, Ni filter (λ = 1.5418 Å), point focusing PolyCap system for parallel beam generation, and 0.3 mm PinHole collimator for the incident beam. Free standing films were investigated with the X-ray perpendicular to the films. The diffraction patterns were recorded with a VÅNTEC-500 area detector using a sample-to-detector distance of 155 mm.

Thin-Film Transistors. The top-gate, bottom-contact organic thin film transistor devices were fabricated on glass substrates (Precision Glass & Optics, Eagle 2000). The gold source and drain electrodes (~35 nm) were deposited by thermal evaporation using a shadow mask (L = 50 μm, W = 500 μm). The polymer was dissolved in the solvent at the concentrations listed in Table 1. The solutions were stirred on a 50 °C hot plate for 2 h in a nitrogen-filled glovebox before use, spin coated at 2000 rpm for 60 s in the glovebox, and followed by annealing on a 110 °C hot plate for 1 h. PMMA dielectric (Sigma-Aldrich, 350 kg/mol, 70 mg/mL in butyl acetate) was spin coated and then annealed at 110 °C for 30 min in the glovebox as well. The PMMA layer thickness was 600−700 nm, resulting in a capacitance of 3.5−4.0 nF/cm^2 as accessed by metal−insulator−metal capacitors (M = Ag, digital capacitance meter, GLK instrument Model 3000). The substrates were cooled to room temperature before being taken out of glovebox for depositing 35 nm gold as the gate electrode. The finished devices were tested in ambient conditions using a Keithley 6430 sub-femtoammeter and a Keithley 2400 source meter, operated by a locally written LabView program and GPIB communication. Mobilities (μ) were calculated in the saturation regime by the standard relationship: $\mu_{sat} = (2I_{DS}L)/[WC_i(V_G-V_T)^2]$, where I_{DS} is the drain−source saturation current, C_i is the gate dielectric capacitance (per area), V_G is the gate voltage, and V_T is the threshold voltage. The latter can be estimated as the x intercept of the linear section of the plot of V_G versus $(I_{DS})^{1/2}$.

ASSOCIATED CONTENT

Supporting Information

Ellipsometry and optical absorption measurements for thickness determination of P-250 and P-23 thin films spin-coated on glass substrates, representative transfer characteristics of FETs prepared by spin-coating, GIWAXS, and DSC data for low MW P(NDI2OD-T2). This material is available free of charge via the Internet at http://pubs.acs.org.

AUTHOR INFORMATION

Corresponding Authors

*E-mail: afacchetti@polyera.com.
*E-mail: tkachov@ipfdd.de.
*E-mail: kiriy@ipfdd.de.

Notes

The authors declare no competing financial interest.

ACKNOWLEDGMENTS

This paper is in honor of the 65th birthday of Prof. Manfred Stamm. We gratefully acknowledge support from the German Excellence Initiative via the Cluster of Excellence EXC 1056 “Center for Advancing Electronics Dresden” (CFAED) and International Helmholtz Research School (IHRS) NanoNet. M.A.H. thanks The University of Jordan and Leibniz-Institut für Polymerforschung (IPF), Dresden, for financial support. T.B. and V.B. thank the Ministry of Education, State Task Project No 4.1626.2014/K for financial support. A.F. thanks KAU for support (grant # 4-130-36-HiCi).

ABBREVIATIONS

MW, molecular weight
FET, field-effect transistor
DSC, differential scanning calorimetry

REFERENCES

(1) Arias, A. C.; MacKenzie, J. D.; McCulloch, I.; Rivnay, J.; Salleo, A. Materials and Applications for Large Area Electronics: Solution-Based Approaches. *Chem. Rev.* **2010**, *110*, 3−24.
(2) Sokolov, A. N.; Tee, B. C.-K.; Bettinger, C. J.; Tok, J. B.-H.; Bao, Z. Chemical and Engineering Approaches to Enable Organic Field-Effect Transistors for Electronic Skin Applications. *Acc. Chem. Res.* **2012**, *45*, 361−371.
(3) Beaujuge, P. M.; Frechet, J. M. J. Molecular Design and Ordering Effects in π-Functional Materials for Transistor and Solar Cell Applications. *J. Am. Chem. Soc.* **2011**, *133*, 20009−200029.
(4) Facchetti, A. π-Conjugated Polymers for Organic Electronics and Photovoltaic Cell Application. *Chem. Mater.* **2010**, *23*, 733−758.
(5) Guo, X.; Facchetti, A.; Marks, T. J. Imide- and Amide-Functionalized Polymer Semiconductors. *Chem. Rev.* **2014**, *114*, 8943−9021.
(6) He, Y.; Hong, W.; Li, Y. New Building Blocks for π-Conjugated Polymer Semiconductors for Organic Thin Film Transistors and Photovoltaics. *J. Mater. Chem. C* **2014**, *2*, 8651−8661.
(7) Li, J.; Zhao, Y.; Tan, H. S.; Guo, Y. L.; Di, C. A.; Yu, G.; Liu, Y. Q.; Lin, M.; Lim, S. H.; Zhou, Y.; Su, H.; Ong, B. S. A Stable Solution-Processed Polymer Semiconductor with Record High-Mobility For Printed Transistors. *Sci. Rep.* **2012**, *2*, 754.
(8) Tsao, H. N.; Cho, D. M.; Park, I.; Hansen, M. R.; Mavrinskiy, A.; Yoon, D. Y.; Graf, R.; Pisula, W.; Spiess, H. W.; Müllen, K. Ultrahigh Mobility in Polymer Field-Effect Transistors by Design. *J. Am. Chem. Soc.* **2011**, *133*, 2605−2612.

DOI: 10.1021/am507759u
ACS Appl. Mater. Interfaces 2015, 7, 12478−12487

(9) Kim, G.; Kang, S.-J.; Dutta, G. K.; Han, Y.-K.; Shin, T. J.; Noh, Y.-Y.; Yang, C. A Thienoisoindigo-Naphthalene Polymer with Ultrahigh Mobility of 14.4 $cm^2/V{\cdot}s$ That Substantially Exceeds Benchmark Values for Amorphous Silicon Semiconductors. *J. Am. Chem. Soc.* **2014**, *136*, 9477−9483.
(10) Yan, H.; Chen, Z.; Zheng, Y.; Newman, C.; Quinn, J. R.; Dötz, F.; Kastler, M.; Facchetti, A. A High-Mobility Electron-Transporting Polymer for Printed Transistors. *Nature* **2009**, *457*, 679−686.
(11) Sun, B.; Hong, W.; Yan, Z.; Aziz, H.; Li, Y. Record High Electron Mobility of 6.3 $cm^2\ V^{-1}\ s^{-1}$ Achieved for Polymer Semiconductors Using a New Building Block. *Adv. Mater.* **2014**, *26*, 2636.
(12) Lei, T.; Xia, X.; Wang, J.-Y.; Liu, C.-J.; Pei, J. "Conformation Locked" Strong Electron-Deficient Poly(p-Phenylene Vinylene) Derivatives for Ambient-Stable n-Type Field-Effect Transistors: Synthesis, Properties, and Effects of Fluorine Substitution Position. *J. Am. Chem. Soc.* **2014**, *136*, 2135−2141.
(13) Horowitz, G.; Hajlaoui, R.; Delannoy, P. Temperature Dependence of the Field-Effect Mobility of Sexithiophene. Determination of the Density of Traps. *J. Phys. III* **1995**, *5*, 355−371.
(14) Asadi, K.; Wu, Y.; Gholamrezaie, F.; Rudolf, P.; Blom, P. W. M. Single-Layer Pentacene Field-Effect Transistors Using Electrodes Modified With Self-Assembled Monolayers. *Adv. Mater.* **2009**, *21*, 4109−4114.
(15) Li, L.; Gao, P.; Schuermann, K. C.; Ostendorp, S.; Wang, W.; Du, C.; Lei, Y.; Fuchs, H.; Cola, L. D.; Mullen, K.; Chi, L. Microribbon Field-Effect Transistors Based on Dithieno[2,3-d;2,3′-d′]benzo[1,2-b;4,5-b′]dithiophene Processed by Solvent Vapor Diffusion. *J. Am. Chem. Soc.* **2010**, *132*, 8807−8809.
(16) Novak, M.; Ebel, A.; Meyer-Friedrichsen, T.; Jedaa, A.; Vieweg, B. F.; Yang, G.; Voitchovsky, K.; Stellacci, F.; Spiecker, E.; Hirsch, A.; Halik, M. Low-Voltage p- and n-Type Organic Self-Assembled Monolayer Field Effect Transistors. *Nano Lett.* **2011**, *11*, 156−159.
(17) Smits, E. C. P.; Mathijssen, S. G. J.; v. Hal, P. A.; Setayesh, S.; Geuns, T. C. T.; Mutsaers, K. A. H. A.; Cantatore, E.; Wondergem, H. J.; Werzer, O.; Resel, R.; Kemerink, M.; Kirchmeyer, S.; Muzafarov, A. M.; Ponomarenko, S. A.; d. Boer, B.; Blom, P. W. M.; d. Leeuw, D. M. Bottom-up Organic Integrated Circuits. *Nature* **2008**, *455*, 956−959.
(18) Sandberg, H. G. O.; Frey, G. L.; Shkunov, M. N.; Sirringhaus, H.; Friend, R. H.; Nielsen, M. M.; Kumpf, C. Ultrathin Regioregular Poly(3-hexyl thiophene) Field-Effect Transistors. *Langmuir* **2002**, *18*, 10176−10182.
(19) Fabiano, S.; Musumeci, C.; Chen, Z.; Scandurra, A.; Wang, H.; Loo, Y.-L.; Facchetti, A.; Pignataro, B. From Monolayer to Multilayer N-Channel Polymeric Field-Effect Transistors with Precise Conformational Order. *Adv. Mater.* **2012**, *24*, 951−956.
(20) Mathijssen, S. G. J.; Smits, E. C. P.; v. Hal, P. A.; Wondergem, H. J.; Ponomarenko, S. A.; Moser, A.; Resel, R.; Bobbert, P. A.; Kemerink, M.; Janssen, R. A. J.; d. Leeuw, D. M. Monolayer Coverage and Channel Length Set the Mobility in Self-Assembled Monolayer Field-Effect Transistors. *Nat. Nanotechnol.* **2009**, *4*, 674−680.
(21) Sizov, A. S.; Agina, E. V.; Gholamrezaie, F.; Bruevich, V. V.; Borshchev, O. V.; Paraschuk, D. Y.; de Leeuw, D. M.; Ponomarenko, S. A. Oligothiophene-Based Monolayer Field-Effect Transistors Prepared by Langmuir−Blodgett Technique. *Appl. Phys. Lett.* **2013**, *103*, 043310.
(22) Scott, J. C.; Samuel, J. D.; Hou, J. H.; Rettner, C. T.; Miller, R. D. Monolayer Transistor Using a Highly Ordered Conjugated Polymer as the Channel. *Nano Lett.* **2006**, *6*, 2916−2919.
(23) Zhang, F.; Di, C.; Berdunov, N.; Hu, Y.; Hu, Y.; Gao, X.; Meng, Q.; Sirringhaus, H.; Zhu, D. Ultrathin Film Organic Transistors: Precise Control of Semiconductor Thickness via Spin-Coating. *Adv. Mater.* **2013**, *25*, 1401−1407.
(24) Zhan, X.; Tan, Z.; An, B.; Domercq, Z.; Zhang, X.; Barlow, S.; Li, Y.; Zhu, D.; Kippelen, B.; Marder, S. R. A High-Mobility Electron-Transport Polymer with Broad Absorption and Its Use in Field-Effect Transistors and All-Polymer Solar Cells. *J. Am. Chem. Soc.* **2007**, *129*, 72467247.
(25) Chen, Z.; Zheng, Y.; Yan, H.; Facchetti, A. Naphthalenedicarboximide- vs Perylenedicarboximide-Based Copolymers. Synthesis and Semiconducting Properties in Bottom-Gate N-Channel Organic Transistors. *J. Am. Chem. Soc.* **2009**, *131*, 8−9.
(26) Schubert, M.; Dolfen, D.; Frisch, J.; Roland, S.; Steyrleuthner, R.; Stiller, B.; Chen, Z.; Scherf, U.; Koch, N.; Facchetti, A.; Neher, D. Influence of Aggregation on the Performance of All-Polymer Solar Cells Containing Low-Bandgap Naphthalenediimide Copolymers. *Adv. Energy Mater.* **2012**, *2*, 369−380.
(27) Moore, J. R.; Albert-Seifried, S.; Rao, A.; Massip, S.; Watts, B.; Morgan, D. J.; Friend, R. H.; McNeill, C. R.; Sirringhaus, H. Polymer Blend Solar Cells Based on a High-Mobility Naphthalenediimide-Based Polymer Acceptor: Device Physics, Photophysics and Morphology. *Adv. Energy Mater.* **2011**, *1*, 230−240.
(28) Steyrleuthner, R.; Schubert, M.; Howard, I.; Klaumünzer, B.; Schilling, K.; Chen, Z.; Saalfrank, P.; Laquai, F.; Facchetti, A.; Neher, D. Aggregation in a High-Mobility n-Type Low-Bandgap Copolymer with Implications on Semicrystalline Morphology. *J. Am. Chem. Soc.* **2012**, *134*, 18303−18317.
(29) Steyrleuthner, R.; Di Pietro, R.; Collins, A. B.; Polzer, F.; Himmelberger, S.; Schubert, M.; Chen, Z.; Zhang, S.; Salleo, A.; Ade, W. H.; Facchetti, A.; Neher, D. The Role of Regioregularity, Crystallinity, and Chain Orientation on Electron Transport in a High-Mobility n-Type Copolymer. *J. Am. Chem. Soc.* **2014**, *136*, 4245−4256.
(30) Fabiano, S.; Hiroyuki, Y.; Chen, Z.; Facchetti, A.; Loi, M. A. Orientation-Dependent Electronic Structures and Charge Transport Mechanisms in Ultrathin Polymeric n-Channel Field-Effect Transistors. *ACS Appl. Mater. Interfaces* **2013**, *5*, 4417−4422.
(31) Kim, T.; Fischer, F. S. U.; Kayunkid, N.; DiPietro, R.; Kiriy, A.; Neher, D.; Ludwigs, S.; Brinkmann, M. Charge Transport Anisotropy in Highly Oriented Thin Films of the Acceptor Polymer P(NDI2OD-T2). *Adv. Energy Mater.* **2014**, *4*, 1301659.
(32) Schmidt, G. C.; Höft, D.; Haase, K.; Hübler, A. C.; Karpov, E.; Tkachov, R.; Stamm, M.; Kiriy, A.; Haidu, F.; Zahn, D.; Yane, H.; Facchetti, A. Naphtalenediimide-Based Donor−Acceptor Copolymer Prepared by Chain-Growth Catalyst-Transfer Polycondensation: Evaluation of Electron-Transporting Properties and Application in Printed Polymer Transistors. *J. Mater. Chem. C* **2014**, *2*, 5149−5154.
(33) Steyrleuthner, R.; Schubert, M.; Jaiser, F.; Blakesley, J. C.; Chen, Z.; Facchetti, A.; Neher, D. Bulk Electron Transport and Charge Injection in a High Mobility n-Type Semiconducting Polymer. *Adv. Mater.* **2010**, *22*, 2799−2803.
(34) Rivnay, J.; Toney, M. F.; Zheng, Y.; Kauvar, I. V.; Chen, Z.; Wagner, V.; Facchetti, A.; Salleo, A. Unconventional Face-On Texture and Exceptional In-Plane Order of a High Mobility n-Type Polymer. *Adv. Mater.* **2010**, *22*, 4359−4363.
(35) Schuettfort, T.; Huettner, S.; Lilliu, S.; Macdonald, J. E.; Thomsen, L.; McNeill, C. R. Surface and Bulk Structural Characterization of a High-Mobility Electron-Transporting Polymer. *Macromolecules* **2011**, *44*, 1530−1539.
(36) Schuettfort, T.; Thomsen, L.; McNeill, C. R. Observation of a Distinct Surface Molecular Orientation in Films of a High Mobility Conjugated Polymer. *J. Am. Chem. Soc.* **2013**, *135*, 1092−1101.
(37) Rivnay, J.; Steyrleuthner, R.; Jimison, L. H.; Casadei, A.; Chen, Z.; Toney, M. F.; Facchetti, A.; Neher, D.; Salleo, A. Drastic Control of Texture in a High Performance n-Type Polymeric Semiconductor and Implications for Charge Transport. *Macromolecules* **2011**, *44*, 5246−5255.
(38) Osaka, I.; McCullough, R. D. Advances in Molecular Design and Synthesis of Regioregular Polythiophenes. *Acc. Chem. Res.* **2008**, *41*, 1202−1214.
(39) Yokozawa, T.; Yokoyama, A. Chain-Growth Condensation Polymerization for the Synthesis of Well-Defined Condensation Polymers and π-Conjugated Polymers. *Chem. Rev.* **2009**, *109*, 5595−5619.
(40) Geng, Y. H.; Huang, L. S.; Wu, P.; Wang, F. S. Kumada Chain-Growth Polycondensation as a Universal Method for Synthesis of

DOI: 10.1021/am507759u
ACS Appl. Mater. Interfaces 2015, 7, 12478−12487

Well-Defined Conjugated Polymers. *Sci. China: Chem.* **2010**, *53*, 1620−1633.
(41) Okamoto, K.; Luscombe, C. K. Controlled Polymerizations for the Synthesis of Semiconducting Conjugated Polymers. *Polym. Chem.* **2011**, *2*, 2424−2434.
(42) Marshall, N.; Sontag, S. K.; Locklin, J. Surface-Initiated Polymerization of Conjugated Polymers. *Chem. Commun.* **2011**, *47*, 15681−16579.
(43) Lanni, E. L.; McNeil, A. Mechanistic Studies on Ni(dppe)Cl_2-Catalyzed Chain-Growth Polymerizations: Evidence for Rate-Determining Reductive Elimination. *J. Am. Chem. Soc.* **2009**, *131*, 16573−16579.
(44) Kiriy, A.; Senkovskyy, V.; Sommer, M. Kumada Catalyst-Transfer Polycondensation: Mechanism, Opportunities and Challenges. *Macromol. Rapid Commun.* **2011**, *32*, 1503−1517.
(45) Tkachov, R.; Senkovskyy, V.; Horecha, M.; Oertel, U.; Stamm, M.; Kiriy, A. Surface-Initiated Kumada Catalyst-Transfer Polycondensation of Poly(9,9-dioctylfluorene) From Organosilica Particles: Chain-Confinement Promoted β-Phase Formation. *Chem. Commun.* **2010**, *46*, 1425−1427.
(46) Komber, H.; Senkovskyy, V.; Tkachov, R.; Johnson, K.; Kiriy, A.; Huck, W. T. S.; Sommer, M. Ring Walking versus Trapping of Nickel(0) during Kumada Catalyst Transfer Polycondensation Using Externally Initiated Electron-Accepting Thiophene−Benzothiadiazole−Thiophene Precursors. *Macromolecules* **2011**, *44*, 9164−9172.
(47) Tkachov, R.; Senkovskyy, V.; Beryozkina, T.; Boyko, K.; Bakulev, V.; Lederer, A.; Sahre, K.; Voit, B.; Kiriy, A. Palladium-Catalyzed Chain-Growth Polycondensation of AB-type Monomers: High Catalyst Turnover and Polymerization Rates. *Angew. Chem., Int. Ed.* **2014**, *53*, 2402−2407.
(48) Yokoyama, A.; Suzuki, H.; Kubota, Y.; Ohuchi, K.; Higashimura, H.; Yokozawa, T. Chain-Growth Polymerization for the Synthesis of Polyfluorene via Suzuki−Miyaura Coupling Reaction from an Externally Added Initiator Unit. *J. Am. Chem. Soc.* **2007**, *129*, 7236−7237.
(49) Beryozkina, T.; Boyko, K.; Khanduyeva, N.; Senkovskyy, V.; Horecha, M.; Oertel, U.; Simon, F.; Stamm, M.; Kiriy, A. Grafting of Polyfluorene by Surface-Initiated Suzuki Polycondensation. *Angew. Chem., Int. Ed.* **2009**, *48*, 2695−2698.
(50) Elmalem, E.; Kiriy, A.; Huck, W. T. S. Chain-Growth Suzuki Polymerization of n-Type Fluorene Copolymers. *Macromolecules* **2011**, *44*, 9057−9061.
(51) Elmalem, E.; Biedermann, F.; Johnson, K.; Friend, R. H.; Huck, W. T. S. Synthesis and Photophysics of Fully π-Conjugated Heterobis-Functionalized Polymeric Molecular Wires via Suzuki Chain-Growth Polymerization. *J. Am. Chem. Soc.* **2012**, *134*, 17769−17777.
(52) Senkovskyy, V.; Tkachov, R.; Komber, H.; Sommer, M.; Heuken, M.; Voit, B.; Huck, W. T. S.; Kataev, V.; Petr, A.; Kiriy, A. Chain-Growth Polymerization of Unusual Anion-Radical Monomers Based on Naphthalene Diimide: A New Route to Well-Defined n-Type Conjugated Copolymers. *J. Am. Chem. Soc.* **2011**, *131*, 19966−19970.
(53) Senkovskyy, V.; Tkachov, R.; Komber, H.; John, A.; Sommer, J.-U.; Kiriy, A. Mechanistic Insight into Catalyst-Transfer Polymerization of Unusual Anion-Radical Naphthalene Diimide Monomers: An Observation of Ni(0) Intermediates. *Macromolecules* **2012**, *5*, 7770−7777.
(54) Liu, W.; Tkachov, R.; Komber, H.; Senkovskyy, V.; Schubert, M.; Neher, D.; Zhao, W.; Facchetti, A.; Kiriy, A. Chain-Growth Polycondensation of Perylene Diimide-Based Copolymers: a New Route to Regio-Regular Perylene Diimide-Based Acceptors for All-Polymer Solar Cells and N-Type Transistors. *Polym. Chem.* **2014**, *5*, 3404−3411.
(55) Tkachov, R.; Komber, H.; Rauch, S.; Lederer, A.; Oertel, U.; Häußler, L.; Voit, B.; Kiriy, A. One-Pot Synthesis of All-Conjugated Block-Like Bisthiophene-Naphthalenediimide/Fluorene Copolymer. *Macromolecules* **2014**, *47*, 4994−5001.
(56) Willot, P.; Moerman, D.; Leclère, P.; Lazzaroni, R.; Baeten, Y.; Auweraer, M.; Koeckelberghs, G. One-Pot Synthesis and Characterization of All-Conjugated Poly(3-alkylthiophene)-block-poly(dialkylthieno[3,4-b]pyrazine). *Macromolecules* **2014**, *47*, 6671−6678.
(57) Bridges, C. R.; McCormick, T. M.; Gibson, G. L.; Hollinger, J.; Seferos, D. S. Designing and Refining Ni(II)diimine Catalysts Toward the Controlled Synthesis of Electron-Deficient Conjugated Polymers. *J. Am. Chem. Soc.* **2013**, *135*, 13212−13219.
(58) Tkachov, R.; Karpov, Y.; Senkovskyy, V.; Raguzin, I.; Zessin, J.; Lederer, A.; Stamm, M.; Voit, B.; Beryozkina, T.; Bakulev, V.; Zhao, W.; Facchetti, A.; Kiriy, A. Efficient Tin-Free Route to a Donor-Acceptor Semiconducting Copolymer with Variable Molecular Weights. *Macromolecules* **2014**, *47*, 3845−3851.
(59) Gasperini, A.; Sivula, K. Effects of Molecular Weight on Microstructure and Carrier Transport in a Semicrystalline Poly(thieno)thiophene. *Macromolecules* **2013**, *46*, 9349−9358.
(60) Zhang, R.; Li, B.; Iovu, M. C.; Jeffries-EL, M.; Sauvé, G.; Cooper, J.; Jia, S.; Tristram-Nagle, S.; Smilgies, D. M.; Lambeth, D. N.; McCullough, R. D.; Kowalewski, T. Nanostructure Dependence of Field-Effect Mobility in Regioregular Poly(3-hexylthiophene) Thin Film Field Effect Transistors. *J. Am. Chem. Soc.* **2006**, *128*, 3480−3481.
(61) Kline, R. J.; McGehee, M. D.; Kadnikova, E.; Liu, J.; Frechet, J. M. J.; Toney, M. F. Dependence of Regioregular Poly(3-hexylthiophene) Film Morphology and Field-Effect Mobility on Molecular Weight. *Macromolecules* **2005**, *38*, 3312−3319.
(62) Zen, A.; Pflaum, J.; Hirschmann, S.; Zhuang, W.; Jaiser, F.; Asawapirom, U.; Rabe, J. P.; Scherf, U.; Neher, D. Effect of Molecular Weight and Annealing of Poly(3-hexylthiophene)s on the Performance of Organic Field-Effect Transistors. *Adv. Funct. Mater.* **2004**, *14*, 757−764.
(63) Zen, A.; Saphiannikova, M.; Neher, D.; Grenzer, J.; Grigorian, S.; Pietsch, U.; Asawapirom, U.; Janietz, S.; Scherf, U.; Lieberwirth, I.; Wegner, G. Effect of Molecular Weight on the Structure and Crystallinity of Poly(3-hexylthiophene). *Macromolecules* **2006**, *39*, 2162−2171.
(64) Schilinsky, P.; Asawapirom, U.; Scherf, U.; Biele, M.; Brabec, C. J. Influence of the Molecular Weight of Poly(3-hexylthiophene) on the Performance of Bulk Heterojunction Solar Cells. *Chem. Mater.* **2005**, *17*, 2175−2180.
(65) Müller, C.; Wang, E.; Andersson, L. M.; Tvingstedt, K.; Zhou, Y.; Andersson, M. R.; Inganäs, O. Influence of Molecular Weight on the Performance of Organic Solar Cells Based on a Fluorene Derivative. *Adv. Funct. Mater.* **2010**, *20*, 2124−2131.
(66) Kline, R. J.; McGehee, M. D.; Kadnikova, E. N.; Liu, J.; Fréchet, J. M. J.; Toney, M. F. Dependence of Regioregular Poly(3-hexylthiophene) Film Morphology and Field-Effect Mobility on Molecular Weight. *Macromolecules* **2005**, *38*, 3312−3319.
(67) Goh, C.; Kline, R. J.; McGehee, M. D.; Kadnikova, E. N.; Fréchet, J. M. Molecular-Weight-Dependent Mobilities in Regioregular Poly-3-hexyl-thiophene Diodes. *J. Appl. Phys. Lett.* **2005**, *86*, 122110.
(68) Ma, W.; Kim, J. Y.; Lee, K.; Heeger, A. J. Effect of the Molecular Weight of Poly(3-hexylthiophene) on the Morphology and Performance of Polymer Bulk Heterojunction Solar Cells. *Macromol. Rapid Commun.* **2007**, *28*, 1776−1780.
(69) Wang, S.; Pisula, W.; Müllen, K. Nanofiber Growth and Alignment in Solution Processed n-type Naphthalene-diimide-Based Polymeric Field-Effect Transistors. *J. Mater. Chem.* **2012**, *22*, 24827−24831.
(70) Kiriy, A.; Stamm, M. Chain Conformation and Manipulation. In *Polymer Science: A Comprehensive Reference*; Matyjaszewski, K., Möller, M., Eds.; Elsevier BV: Amsterdam, The Netherlands, 2012; Vol. *1*, pp 367−386.
(71) Kiriy, N.; Jähne, E.; Adler, H.− J.; Schneider, M.; Kiriy, A.; Gorodyska, G.; Minko, S.; Jehnichen, D.; Simon, P.; Fokin, A. A.; Stamm, M. One-Dimensional Aggregation of Regioregular Polyalkylthiophenes. *Nano Lett.* **2003**, *3*, 707−712.
(72) Kiriy, A.; Gorodyska, A.; Minko, S.; Jaeger, W.; Štěpánek, P.; Stamm, M. Cascade of Coil-Globule Conformational Transitions of Single Flexible Polyelectrolyte Molecules in Poor Solvent. *J. Am. Chem. Soc.* **2002**, *124*, 13454−13462.

DOI: 10.1021/am507759u
ACS Appl. Mater. Interfaces 2015, 7, 12478−12487

(73) Noriega, R.; Rivnay, J.; Vandewal, K.; Koch, F. P. V.; Stingelin, N.; Smith, P.; Toney, M. F.; Salleo, A. A General Relationship Between Disorder, Aggregation and Charge Transport in Conjugated Polymers. *Nat. Mater.* **2013**, *12*, 1038−1044.
(74) Kline, R. J.; McGehee, M. d.; Kadnikova, E. n.; Liu, J.; Fréchet, J. Controlling the Field-Effect Mobility of Regioregular Polythiophene by Changing the Molecular Weight. *Adv. Mater.* **2003**, *15*, 1519−1522.

DOI: 10.1021/am507759u
ACS Appl. Mater. Interfaces 2015, 7, 12478−12487